ESC European Society of Cardiology

Europace (2023) **25**, 1–12
https://doi.org/10.1093/europace/euad197

TRANSLATIONAL RESEARCH

Body surface potential mapping detects early disease onset in *plakophilin-2*-pathogenic variant carriers

Manon Kloosterman [1]*, Machteld J. Boonstra [1], Rob W. Roudijk [1], Mimount Bourfiss [1], Iris van der Schaaf[1], Birgitta K. Velthuis [2], Thijs M. H. Eijsvogels [3], Feddo P. Kirkels [1], Peter M. van Dam [1,4], and Peter Loh [1]

[1]Department of Cardiology, University Medical Center Utrecht, Utrecht, The Netherlands; [2]Department of Radiology, University Medical Center Utrecht, Utrecht, The Netherlands; [3]Department of Physiology, Radboud University Medical Center, Nijmegen, The Netherlands; and [4]ECG-Excellence BV, Nieuwerbrug, The Netherlands

Received 19 March 2023; accepted after revision 4 July 2023; online publish-ahead-of-print 11 July 2023

Aims Arrhythmogenic right ventricular cardiomyopathy (ARVC) is a progressive inherited cardiac disease. Early detection of disease and risk stratification remain challenging due to heterogeneous phenotypic expression. The standard configuration of the 12 lead electrocardiogram (ECG) might be insensitive to identify subtle ECG abnormalities. We hypothesized that body surface potential mapping (BSPM) may be more sensitive to detect subtle ECG abnormalities.

Methods and results We obtained 67 electrode BSPM in *plakophilin-2* (*PKP2*)-pathogenic variant carriers and control subjects. Subject-specific computed tomography/magnetic resonance imaging based models of the heart/torso and electrode positions were created. Cardiac activation and recovery patterns were visualized with QRS- and STT-isopotential map series on subject-specific geometries to relate QRS-/STT-patterns to cardiac anatomy and electrode positions. To detect early signs of functional/structural heart disease, we also obtained right ventricular (RV) echocardiographic deformation imaging. Body surface potential mapping was obtained in 25 controls and 42 *PKP2*-pathogenic variant carriers. We identified five distinct abnormal QRS-patterns and four distinct abnormal STT-patterns in the isopotential map series of 31/42 variant carriers. Of these 31 variant carriers, 17 showed no depolarization or repolarization abnormalities in the 12 lead ECG. Of the 19 pre-clinical variant carriers, 12 had normal RV-deformation patterns, while 7/12 showed abnormal QRS- and/or STT-patterns.

Conclusion Assessing depolarization and repolarization by BSPM may help in the quest for early detection of disease in variant carriers since abnormal QRS- and/or STT-patterns were found in variant carriers with a normal 12 lead ECG. Because electrical abnormalities were observed in subjects with normal RV-deformation patterns, we hypothesize that electrical abnormalities develop prior to functional/structural abnormalities in ARVC.

* Corresponding author. Tel: +31 088 75 57008. *E-mail address*: manon.kloosterman@live.com

© The Author(s) 2023. Published by Oxford University Press on behalf of the European Society of Cardiology.
This is an Open Access article distributed under the terms of the Creative Commons Attribution-NonCommercial License (https://creativecommons.org/licenses/by-nc/4.0/), which permits non-commercial re-use, distribution, and reproduction in any medium, provided the original work is properly cited. For commercial re-use, please contact journals.permissions@oup.com

Graphical Abstract

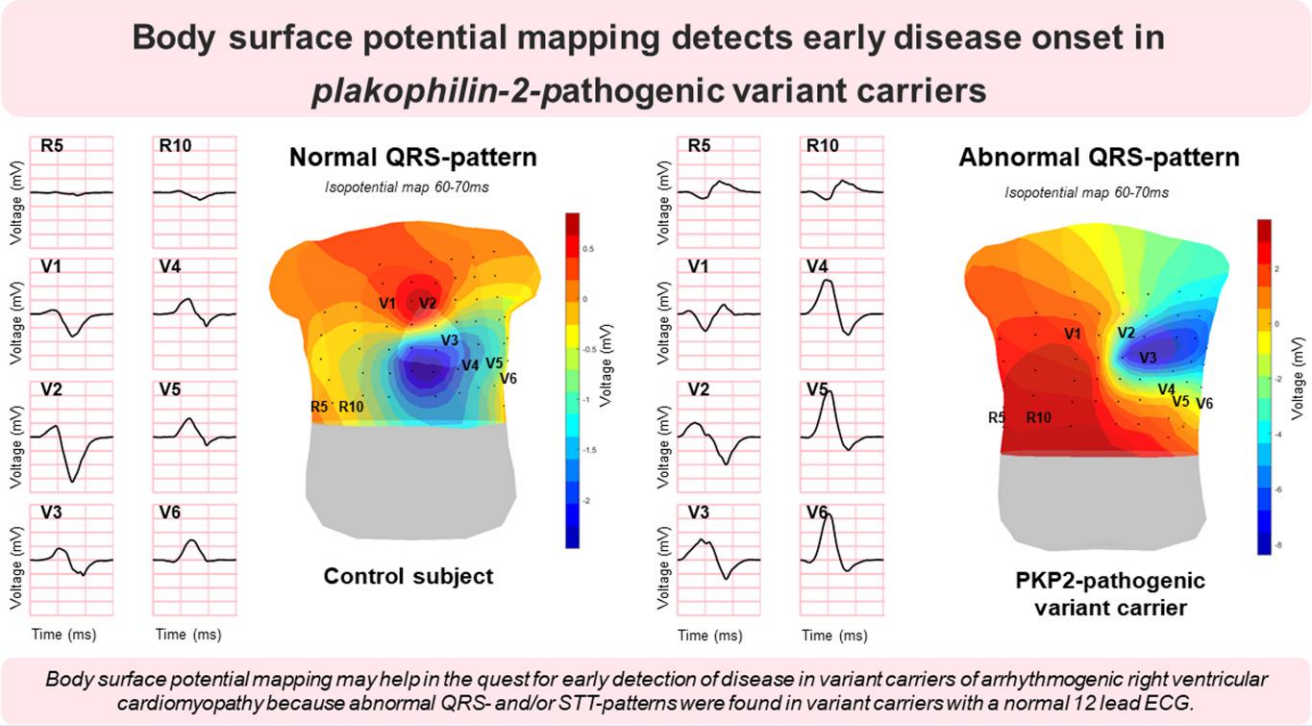

Keywords Arrhythmogenic right ventricular cardiomyopathy • Plakophilin-2 • Body surface potential mapping • Isopotential map series

Translational perspective

We observed depolarization and repolarization abnormalities by body surface potential mapping in pathogenic *plakophilin-2* variant carriers with a normal 12 lead electrocardiogram and normal deformation patterns of the right ventricular lateral wall. This indicates that body surface potential mapping is able to detect the presence of an early stage of disease. Hence, body surface potential mapping can be used for serial measurements to investigate early disease onset and progression and to correlate these electrocardiographic changes to clinical outcome measures such as ventricular arrhythmias. These findings may improve risk stratification and prevention of life-threatening arrhythmias.

What's new?

- Identification of abnormal isopotential map patterns in *PKP2*-pathogenic variant carriers with a normal 12 lead ECG.
- Observation of ECG abnormalities in *PKP2*-pathogenic variant carriers outside the standard 12 lead ECG positions.
- Observation of abnormal isopotential map patterns in *PKP2*-pathogenic variant carriers with normal right ventricular deformation patterns.

Introduction

Arrhythmogenic right ventricular cardiomyopathy (ARVC) is defined as a progressive genetic heart muscle disease characterized by fibrofatty myocardial replacement predominantly affecting the right ventricle (RV). Most of the pathogenic variants have been identified in genes encoding desmosomal proteins. Because a desmosomal protein is part of the intercalated disk, a genetic variant in the desmosomes may lead to redistribution of other intercalated disk proteins, resulting in mechanical and electrical uncoupling of cardiac myocytes. This mechanism is hypothesized to induce cell death and inflammation resulting in fibrofatty myocardial replacement. However, the described electromechanical uncoupling may occur in the absence of structural heart disease. Therefore, life-threatening ventricular arrhythmias can occur in still asymptomatic patients.[1,2] Early detection of disease in these asymptomatic variant carriers is therefore of utmost importance to prevent sudden cardiac death.[3]

Early detection and risk stratification in ARVC is complicated by heterogeneous phenotypic expression. This wide range in disease manifestation is also represented in the current guidelines to diagnose ARVC, the Task Force Criteria (TFC). Rather than using one single diagnostic test, the diagnosis is based on the TFC that includes structural, histological, electrocardiographic (ECG), arrhythmic, and familial features.[4] To this day, the complex interplay of genetic predisposition and environmental factors resulting in ARVC manifestation are only partially unravelled.[5] ARVC diagnosis is further complicated because imaging of the RV is challenging due to the thin RV wall and low specificity of ECG abnormalities.[2] Therefore, there is a need for a sensitive diagnostic technique to improve identification of early disease in ARVC.[3]

Recently, echocardiographic deformation imaging has been described to play a potential prognostic role in the identification of early myocardial involvement in ARVC. Mast *et al.*[6] described abnormal deformation patterns in the RV basal area of ARVC desmosomal variant carriers without electrical or structural abnormalities according to the 2010 TFC. The absence of ECG abnormalities is striking since increasing evidence suggests that electrical changes develop prior to structural abnormalities.[5] However, the standard configuration of the 12 lead ECG might be insensitive to identify subtle ECG abnormalities. To detect these subtle depolarization and repolarization abnormalities, it is suggested to use 67 electrode body surface potential mapping (BSPM).

In this study, we aimed to explore novel ECG depolarization and repolarization patterns in plakophilin-2 (*PKP2*)-pathogenic variant carriers using 67 electrode BSPM. The 67 electrode BSPM was combined with patient-specific 3D anatomical models to relate cardiac activation and recovery patterns to cardiac anatomy and electrode positions. Besides BSPM, we also obtained RV deformation patterns to detect early signs of functional/structural heart disease in the RV basal area. We hypothesized that BSPM may be a more sensitive method to detect electrical abnormalities in the RV compared to the standard 12 lead ECG.

Methods

Study population

Subjects with definite ARVC (TFC $\geq$ 4), borderline ARVC (TFC = 3), and pre-clinical subjects carrying a pathogenic *PKP2* variant (TFC = 2) who were clinically referred for cardiac magnetic resonance imaging (MRI) in the University Medical Center Utrecht were included in the ARVC population of this study. Besides cardiac MRI, all subjects underwent standard diagnostic evaluation for ARVC including a standard 12 lead ECG, 24 h Holter monitoring and echocardiography. Signal-averaged ECG and biopsies were not routinely performed in our center and therefore not part of this study.

The control group was a mixed population of subjects who were clinically referred for cardiac MRI in the University Medical Center Utrecht and recreational marathon athletes who underwent cardiac MRI for study purposes.[7] Subjects were included in the control population if no functional/structural heart disease was present at echo/MRI, no cardiovascular diseases or risk factors were present, and QRS duration was <120 ms. Studies were approved by the local institutional ethics review board at University Medical Center Utrecht (ID: 17/628) and Amsterdam University Medical Centers (ID: NL61873.018.17).

Body surface potential mapping signal acquisition and processing

Each subject underwent 67 electrode BSPM (sampling frequency = 2048Hz, Biosemi, Amsterdam, The Netherlands) within 32 days before/after cardiac MRI. Nine electrodes were placed on the back and 55 on the chest using 12 vertical strips of 28 cm with 4 cm between adjacent electrodes. All electrodes were referenced to Wilson's Central Terminal derived from the limb leads. Body surface potential mapping was recorded for ~5 min with the patient in resting supine position. Recreational marathon athletes underwent BSPM 1 week prior to the marathon.

BSPM signals were loaded into MATLAB (R2019B) for offline processing and signal analysis. Signals were down sampled to 1000 Hz, high-pass filtered (fc = 0.25 Hz), low-pass filtered (fc = 200 Hz), and notch filtered (50 Hz). Ten beats with the most identical morphology and maximal RS amplitude (assumed end-expiration) were selected and used to compute a median beat. The root mean square signal calculated with all 67 leads was used to manually annotate QRS-onset and QRS-end. The beginning of repolarization (T-onset) was manually annotated, and the end of repolarization (T-end) was determined based on a previously described integration operation method.[8] Leads containing electrode motion artefacts were removed or linearly interpolated.

Cardiac magnetic resonance imaging acquisition and processing

All subjects underwent cardiac MRI (Philips Medical System, Achieva, Best, the Netherlands). Segmentation was performed on cardiac short-axis and long-axis Cine MRI images at end diastole. Per subject, obtained cardiac MRI was used to create a 3D model of the ventricular myocardium and torso. Images were segmented using dedicated software and discretized as closed triangulated surface meshes bounding the segmented mass (GeomPeacs, Version 0.1.1.4408, Peacs Investments BV).[9] Lead positions were captured using a 3D camera during the BSPM and registered to the torso model (PeacsCamera, Version 0.02.4979, Peacs Investments BV).[10]

Echocardiographic deformation imaging acquisition and processing

Echocardiography was performed during follow-up of *PKP2*-pathogenic variant carriers. In 93% of the *PKP2*-pathogenic variant carriers, echocardiography was performed 2.5 months before or after BSPM. We performed echocardiography, using a GE Vivid E9 or E95 scanner (GE Healthcare, Horten, Norway). Cine loops were stored for post-processing with EchoPac version 203 (GE Healthcare). Details on acquisition of the RV-focused four chamber view and post-processing in echocardiographic speckle tracking deformation imaging were previously described more extensively.[11] RV deformation patterns were assessed to detect early signs of functional/structural disease. We focused on the RV basal area, since this was the earliest and most severely affected area in previous studies in *PKP2*-variant carriers.[6,12,13] Deformation patterns of the RV basal lateral wall were classified into type I (normal deformation), type II (slightly abnormal deformation), or type III (severely abnormal deformation), based on the classification method proposed by Mast *et al.*[12]

Isopotential map series

The workflow for the computation of the isopotential map series is displayed in *Figure 1*. First, the BSPM data were used to compute 2D isopotential map series. For this purpose, the QRS- and STT-segments were divided into smaller time intervals of 5 ms. Then, for each time interval within the QRS- and STT-segment, the average potential value over five samples was calculated. This was performed for all 67 signals resulting in a potential value for each electrode. Subsequently, the potential values were displayed on a 2D representation of the torso where equal potential values (isopotentials) were connected with lines. The 2D isopotential map series were then combined with a 3D subject-specific geometry to create subject-specific 3D isopotential map series. The potential values at the location of electrodes were used for surface Laplacian interpolation to construct the isopotential map series for the complete torso surface.

QRS- and STT-isopotential map series of all control subjects were visually evaluated by two observers to define a normal isopotential map pattern. To define normal QRS-patterns, the locations, timings, and durations of the minima and maxima were assessed for all 5 ms intervals. To define normal STT-patterns, only the locations of the minima and maxima were assessed for all 5 ms intervals. Based on the observed locations (and timings and durations) of minima and maxima in the normal QRS- and STT-isopotential maps, QRS- and STT-isopotential maps of *PKP2*-pathogenic variant carriers were classified abnormal if local minima or maxima appeared outside the normal locations, timings, or durations.

Isopotential map series compared to 2010 Task Force Criteria

Per subject, 2010 TFC were scored and baseline characteristics such as sex, age, and QRS duration were determined. Data were presented as *n* (%) or median and the 25th percentile (Q1) and 75th percentile (Q3). QRS- and STT-isopotential map series of *PKP2*-pathogenic variant carriers were compared to the presence of 2010 TFC as reported in the clinical record during the time of the BSPM. The association between ECG 2010 TFC abnormalities (terminal activation duration (TAD) of QRS $\geq$ 55 ms and inverted T-waves) on 12 lead ECG and QRS-/STT-patterns on BSPM was tested using a χ^2 or Fisher's exact test, as appropriate. A *P*-value <0.05 was considered statistically significant.

Results

The study population (*Table 1*) consisted of 67 individuals, of whom 25 control subjects and 42 *PKP2*-pathogenic variant carriers. The control

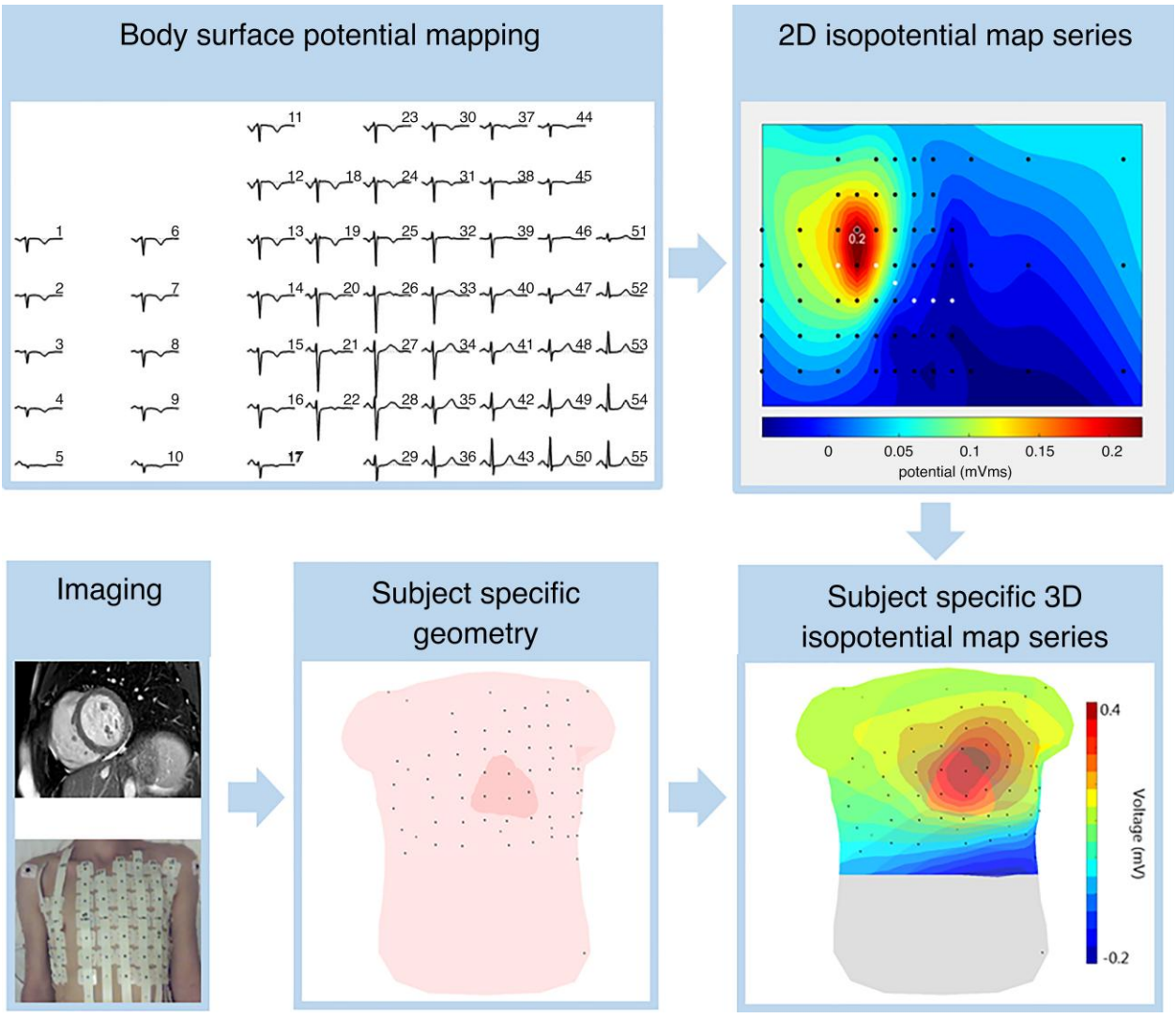

Figure 1 Workflow for the computation of subject-specific 3D isopotential map series. Cardiac imaging (magnetic resonance imaging/computed tomography) and 3D images of electrode positions are used to create a subject-specific geometry. This subject-specific geometry is combined with 2D isopotential map series, derived from 67 electrode body surface potential mapping, to create subject-specific isopotential map series. In the isopotential map series, the average potential value within 5 ms of the QRS complex is displayed. Dark red indicates the absolute maximum, dark blue the absolute minimum. Potential values in between are colored as indicated in the color scale. The isochrones are spaced with equal potential values.

population without detectable structural or functional heart disease consisted of seven (28%) subjects undergoing electrophysiological study for premature ventricular complexes from the RV outflow tract (RVOT-PVC), three (12%) subjects with non-cardiac chest pain, and 15 recreational athletes (60%). Three of the patients with RVOT-PVC underwent a radiofrequency catheter ablation. The population of *PKP2*-pathogenic variant carriers consisted of 14 patients with definite ARVC (TFC $\geq$ 4), 9 subjects with borderline ARVC (TFC = 3), and 19 pre-clinical subjects (TFC = 2).

Normal QRS-isopotential map series

In a representative example of the QRS-isopotential map series in a control subject (*Figure 2*), the first maximum (red area) appeared at the chest above the mid or upper part of the heart (0–9 ms). Thereafter, the position of the maximum moved over the chest, towards a position near the apex of the heart (10–34 ms), whereafter it moved to the back (35–64 ms). At the end of depolarization, the maximum remained on the back or appeared above the RVOT (70–79 ms). The first minimum (blue area) was located on the back (0–19 ms) and moved towards the right superior area of the chest (20–24 ms). The minimum then moved towards the location where initially a maximum was located (35–44 ms) and thereafter towards the area on the chest above the mid/apical part of the RV (45–79 ms). The observed locations of maxima and minima and their corresponding appearance in time and duration in the complete control population are presented in *Table 2*.

Abnormal QRS-isopotential maps

Five abnormal QRS-patterns were distinguished in 25/42 (60%) *PKP2*-pathogenic variant carriers (*Table 1*). An abnormal timing

Table 1 Baseline characteristics, QRS- and STT-isopotential map patterns, and RV deformation patterns

	Control subjects ($n = 25$)	Pre-clinical variant carriers ($n = 19$)	Borderline ARVC ($n = 9$)	Definite ARVC ($n = 14$)
Age (years)	50 (35; 55)	27 (21; 43)	34 (30; 57)	51 (29; 62)
Male	13 (52)	12 (63)	4 (44)	8 (57)
QRS duration (ms)	91 (85; 96)	87 (81; 99)	100 (91; 106)	97 (87; 110)
2010 TFC				
Global or regional dysfunction and structural alterations	0 (0)	0 (0)	0 (0)	12 (86)
Repolarization abnormalities	0 (0)	0 (0)	0 (0)	9 (64)
Depolarization abnormalities	0 (0)	0 (0)	5 (56)	5 (36)
Arrhythmias	0 (0)	0 (0)	4 (44)	14 (100)
Family history	0 (0)	19 (100)	9 (100)	14 (100)
QRS-isopotential map pattern				
A	0 (0)	5 (26)	2 (22)	4 (29)
B	0 (0)	1 (5)	0 (0)	1 (7)
C	0 (0)	4 (21)	2 (22)	2 (14)
D	0 (0)	0 (0)	0 (0)	3 (21)
E	0 (0)	1 (5)	0 (0)	1 (7)
STT-isopotential map pattern				
A	0 (0)	2 (11)	2 (22)	1 (7)
B	0 (0)	1 (5)	0 (0)	0 (0)
C	0 (0)	0 (0)	1 (11)	10 (71)
D	0 (0)	0 (0)	0 (0)	7 (50)
RV deformation pattern[a]				
I	19 (95)	12 (63)	4 (44)	3 (21)
II	1 (5)	7 (37)	5 (56)	4 (29)
III	0 (0)	0 (0)	0 (0)	7 (50)

Categorical variables are displayed as *n* (%), continuous variables as median (Q1; Q3). ARVC diagnosis is fulfilled in the presence of two major, one major, and two minor or four minor 2010 TFC. QRS- and STT-isopotential map patterns are defined as indicated in *Figures 3* and *5*, respectively. RV deformation imaging was assessed using speckle tracking echocardiography. ARVC, arrhythmogenic right ventricular cardiomyopathy; TFC, Task Force Criteria; RV, right ventricular; BSPM, body surface potential mapping.

[a]The RV echocardiographic deformation control population consisted of other individuals then the BSPM control population. The median age of this population was 28 years (Q1: 22; Q3: 33), 53% were men, and the QRS duration was within the normal range [95 ms (Q1: 88; Q3: 103)].

and/or location of the maximum in the leads positioned at the right side of the chest (*Figure 3*, QRS-pattern A/B/C) was most commonly observed (84%). In detail, we observed a maximum at the right distal part of the chest ranging from 51 to 143 ms after QRS onset. The location of this maximum was not observed in any control subject and was defined as abnormal QRS-pattern A. The second abnormality was a late appearance of the maximum above the basal part of the heart, 28–38 ms after QRS onset compared to 0–26 ms after QRS onset in the control population (*Table 2*). The late appearance of this maximum was defined as abnormal QRS-pattern B. We also observed an abnormal duration of the maximum above the RV outflow tract, >45 ms compared to 35 ms in the control population (*Table 2*). The long duration of this maximum was defined as abnormal QRS-pattern C. Furthermore, we observed the appearance of a minimum at the left proximal side of the chest instead of the right proximal side of the chest as observed in controls subjects. The abnormal location of this minimum was defined as abnormal QRS-pattern D. Another observed abnormality was the presence of two minima instead of one minimum in the control population. The appearance of these minima was defined as abnormal QRS-pattern E.

Normal STT-isopotential maps

During repolarization in a representative control subject (*Figure 4*), the maximum was located at the left distal area of the chest (around the apex of the heart), and the minimum was located at the right proximal area of the chest (around the RVOT). During repolarization, potential values increased and decreased, but their locations did not change much.

Abnormal STT-isopotential maps

Four abnormal STT-patterns (*Figure 5*) were distinguished in 17/42 (40%) *PKP2*-pathogenic variant carriers (*Table 1*). Six subjects showed a similar repolarization pattern as observed in the control population, but the maximum on the chest was shifted towards the RV basal segment (*Figure 5*, STT-pattern A). A second maximum at the right distal side of the back during repolarization was observed in one subject (*Figure 5*, STT-pattern B). Eleven other subjects showed an abnormal minimum (*Figure 5*, STT-pattern C). Instead of a minimum located at the right upper part of the chest, the minimum was located elsewhere, e.g. at the left distal side of the chest. Of these 11 subjects, seven subjects showed not only one minimum but two or three minima and maxima (*Figure 5*, STT-pattern D).

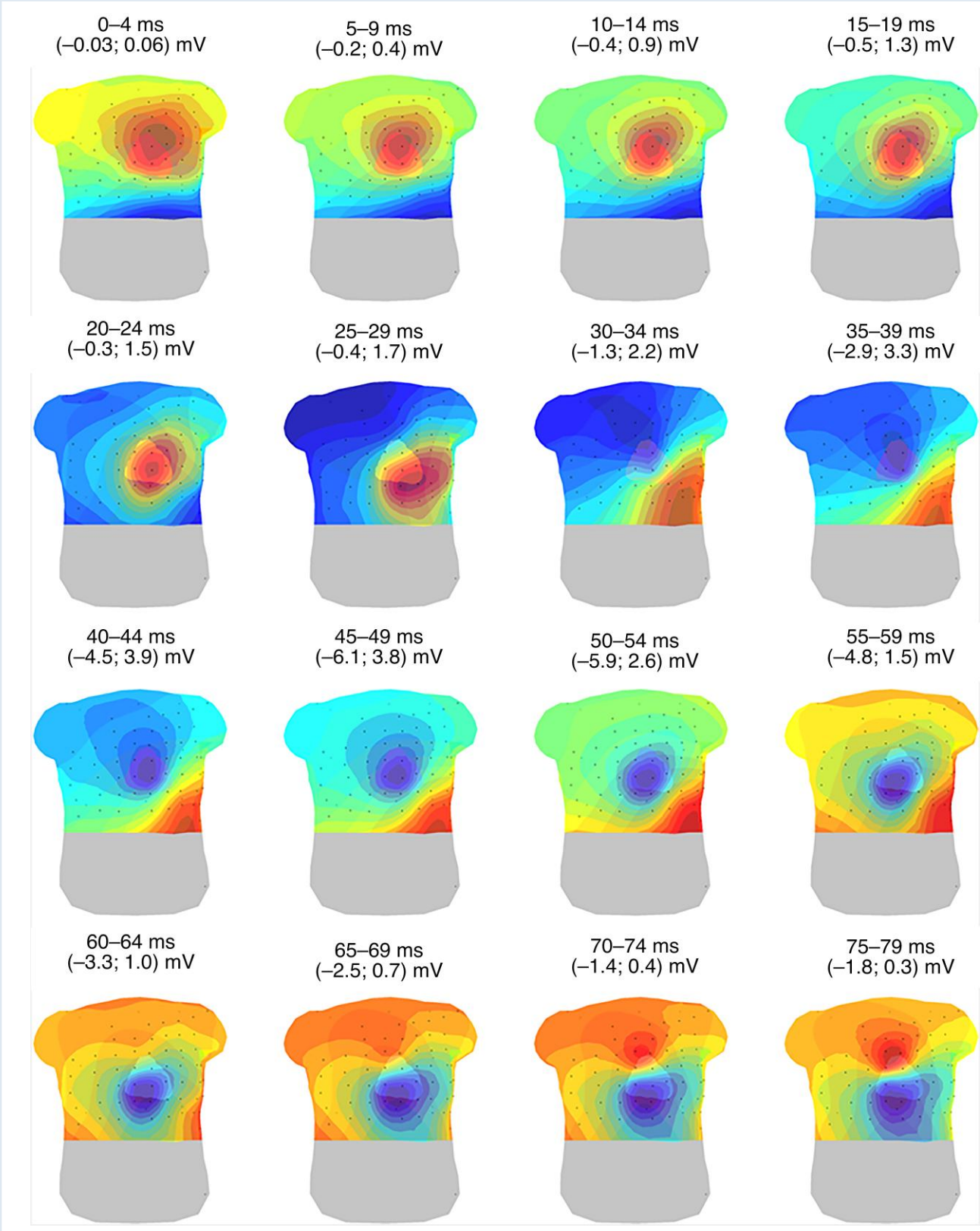

Figure 2 Representative example of the QRS-isopotential map series in a control subject. Isopotential map series of a control subject are displayed on a 3D model of the heart and torso (anterior view) with electrodes (black dots) for 16 intervals of 5 ms within the QRS-complex. Dark red indicates the absolute maximum, dark blue the absolute minimum per time interval. The isochrones are spaced with equal potential values.

Task Force Criteria-based arrhythmogenic right ventricular cardiomyopathy stage classification and abnormal QRS- and STT-patterns

TFC-based ARVC stage classification in the PKP2-pathogenic variant carriers is summarized in *Table 1*; a detailed description per patient can be found in Supplementary material online, *Table S1*. In the pre-clinical variant carriers, 10/19 showed an abnormal QRS-pattern and 3/19 an abnormal STT-pattern. Four of nine patients with borderline ACM showed an abnormal QRS-pattern and three an abnormal STT-pattern. An abnormal QRS- and STT-pattern was observed in 10/14 definite ACM patients, two subjects showed an abnormal QRS- or STT-pattern, and two other subjects showed no abnormal patterns. QRS-patterns A–C and E were observed in all TFC-based ARVC stadia and abnormal QRS-pattern D only in definite ARVC patients. Abnormal STT-pattern A was observed in all TFC-based ARVC stadia, abnormal STT-pattern B in a pre-clinical variant carrier, and STT-patterns C and D were only observed in definite ACM patients, except for one patient with borderline ARVC showing abnormal STT-pattern C.

Table 2 Maxima and minima with corresponding timings and durations in the isopotential map series during depolarization of control subjects

Location of maxima	Time interval[a]	Location of minima	Timing[a]
Base (heart)	0–26 (26)	Left anterior torso	0–26 (26)
Mid (heart)	0–32 (20)	Posterior torso	0–32 (26)
Apex (heart)	0–86 (68)	Right anterior torso	3–59 (32)
Posterior torso	33–90 (51)	Above the heart (apex/mid/base)	12–98 (71)
Right ventricular outflow tract	45–98 (35)		

[a]Time intervals are displayed as the interval of occurrence (maximal observed duration). A representative example of the observed locations of maxima and minima during depolarization and the corresponding time intervals are presented in *Figure 2*.

Task Force Criteria fulfilment and abnormal QRS- and STT-patterns

Fulfilment of 2010 TFC in the *PKP2*-pathogenic variant carriers is summarized in *Table 1*; a detailed description per patient can be found in Supplementary material online, *Table S1*. In 17/42 *PKP2*-pathogenic variant carriers, abnormal QRS- and/or STT-patterns were observed, while no depolarization or repolarization abnormalities (2010 TFC) were observed in the 12 lead ECG. Depolarization or repolarization abnormalities (2010 TFC) were observed in the 12 lead ECG in 15/42 *PKP2*-pathogenic variant carriers. Seven of 21 *PKP2*-pathogenic variant carriers, showing an abnormal timing and/or location of the maximum in the leads positioned at the right side of the chest (*Figure 3*, QRS-pattern A/B/C), had a TAD of QRS ≥ 55 ms in V1, V2, or V3 in

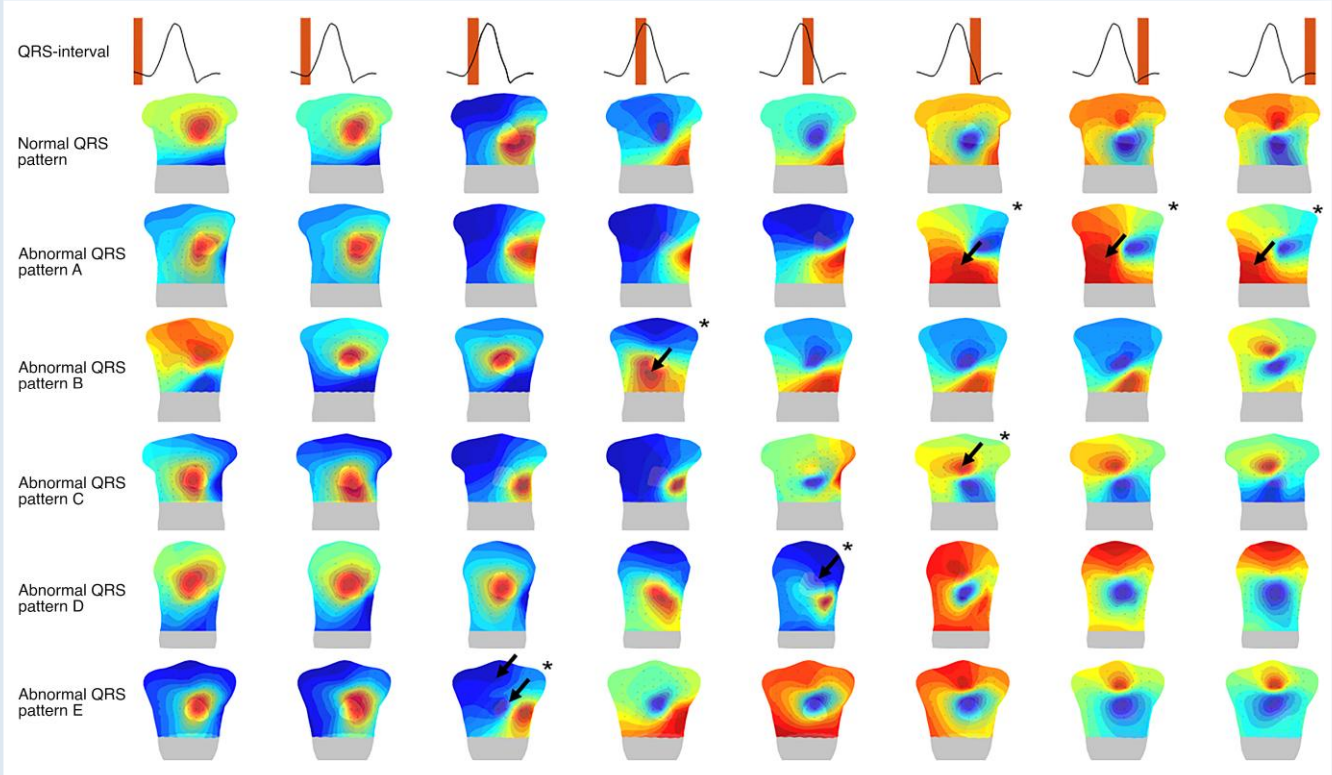

Figure 3 Abnormal QRS-patterns in pathogenic plakophilin-2 variant carriers. Isopotential map series are displayed on a 3D model of the heart and torso (anterior view) with electrodes (black dots) for eight intervals within the QRS-complex (upper row). A representative sample of a normal QRS-isopotential map pattern is displayed in row two. Rows three to seven are representative examples of the five abnormal (black arrows and asterisk) observed QRS-patterns (*A*–*E*) in the plakophilin-2 population. Dark red indicates the absolute maximum, dark blue the absolute minimum. The isochrones are spaced with equal potential values.

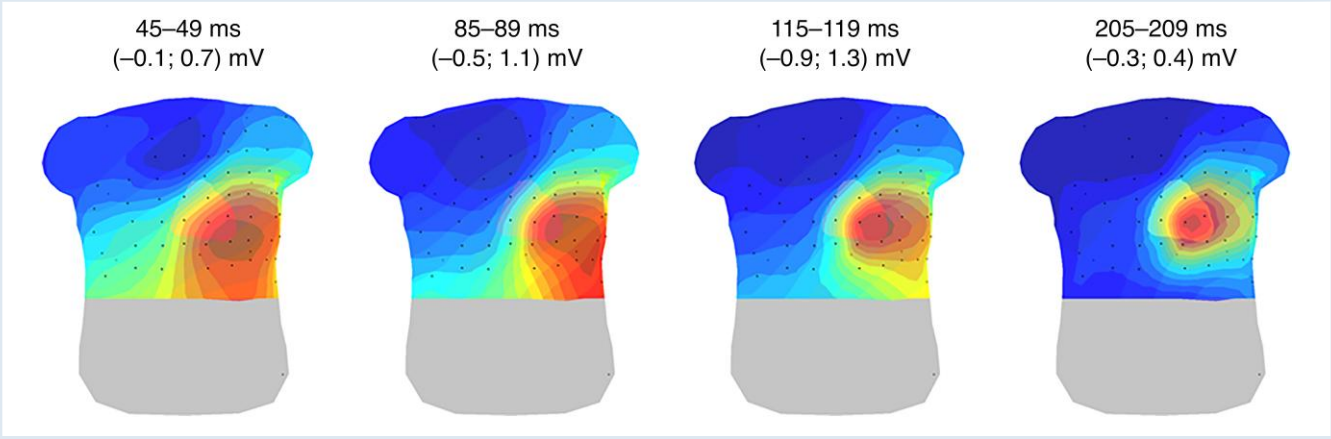

Figure 4 Representative example for the STT-isopotential map series in a control subject. Four intervals of 5 ms are displayed representing the distinct phases during repolarization. Dark red indicates the absolute maximum, dark blue the absolute minimum per time interval, representing an apex to base direction for the repolarization. The isochrones are spaced with equal potential values. Black dots represent the electrode positions.

the 12 lead ECG. All subjects showing QRS-pattern D had a minor or major criterion on imaging. Of the 11 subjects showing STT-pattern C, eight had a minor or major criterion on repolarization abnormalities. Seven of 11 subjects showing STT-pattern C also showed STT-pattern D. Of these seven subjects showing STT-pattern D, six subjects had a history of sustained ventricular arrhythmias.

Twelve-lead electrocardiogram and 67 lead body surface potential mapping

Overall, the presence of abnormal QRS- and/or STT-patterns on the BSPM was associated with the presence of depolarization and/or repolarization abnormalities (2010 TFC) on the 12 lead ECG ($P < 0.05$). An example of two *PKP2*-pathogenic variant carriers without definite ARVC diagnosis showing an abnormal QRS- or STT-pattern is presented in *Figure 6*. QRS-pattern A was observed in a pre-clinical subject with no depolarization or repolarization abnormalities in the 12 lead ECG (*Figure 6*, panel A). The other subject was classified with borderline ARVC based on the presence of TAD of QRS $\geq$ 55 ms in V1, V2, or V3 (ECG). No other depolarization or repolarization abnormalities (2010 TFC) could be observed in the 12 lead ECG. In the BSPM of this patient, negative T-waves could be observed below the precordial leads V4–V6 (*Figure 6*, panel B).

Body surface potential mapping and echocardiographic right ventricular deformation imaging

Of the *PKP2*-pathogenic variant carriers, 19 subjects were classified with a normal type I RV basal deformation pattern, 16 subjects with a type II RV basal deformation pattern, and seven subjects with a type III RV basal deformation pattern (*Table 1*). Two pre-clinical and one borderline *PKP2*-pathogenic variant carriers with abnormal RV basal deformation patterns showed normal QRS- and STT-patterns. On the other hand, seven pre-clinical and three borderline *PKP2*-pathogenic variant carriers with normal RV basal deformation patterns, showed abnormal QRS- and/or STT-patterns. Of the definite ARVC patients with normal QRS- and/or STT-patterns, one subject showed a type II RV deformation pattern, while two ARVC patients with an abnormal QRS- and/or STT-pattern showed a type I RV deformation pattern.

Discussion

This study combined patient-specific 3D anatomical models with BSPM to identify subtle ECG abnormalities using isopotential map series in a broad spectrum of *PKP2*-pathogenic variant carriers. We hypothesized that BSPM is able to detect early electrical abnormalities, even in the absence of depolarization/repolarization TFC on the 12 lead ECG. We observed five distinct abnormal QRS-patterns and four distinct abnormal STT-patterns in the isopotential map series of 74% of the *PKP2*-pathogenic variant carriers. In 17/42 *PKP2*-pathogenic variant carriers with an abnormal BSPM, no depolarization or repolarization abnormalities (2010 TFC) were observed in the 12 lead ECG. Also, 7/12 pre-clinical *PKP2*-pathogenic variant carriers showing abnormal QRS- and/or STT-patterns showed normal RV basal deformation patterns. Because electrical abnormalities were found in subjects with normal RV basal deformation patterns, the predilection area in ARVC, we hypothesize that electrical abnormalities develop prior to functional/structural abnormalities. Therefore, BSPM might help in the quest for early detection of disease onset in *PKP2*-pathogenic variant carriers.

Body surface potential mapping analysis methods

The locations and timings of minima and maxima in the normal QRS- and STT-isopotential maps of our study are similar to the normal isopotential map series described in other studies.[14,15] To our knowledge, this study is the first using isopotential map series in a population of ARVC-related variant carriers. Body surface potential mapping combined with patient-specific 3D anatomical models enabled us to relate cardiac activation and recovery patterns to cardiac anatomy and electrode positions. Using this novel approach, abnormal QRS- and STT-patterns were identified in 74% of the *PKP2*-pathogenic variant carriers, mainly related to abnormal RV activation/recovery.

Previous studies using BSPM were mainly focused on patients with definite ARVC.[16,17] These studies computed isopotential maps over the complete QRS- or QRST-complex. For the computation of these QRS- or QRST-isopotential maps, the area under the QRS- or QRST-complex is approximated for each lead. Then, the potential values are displayed on a 2D representation of the torso. A major drawback of this method is that subtle pathological waveforms over a period of 10 or 20 ms may be lost and/or concealed by the S-wave resulting in

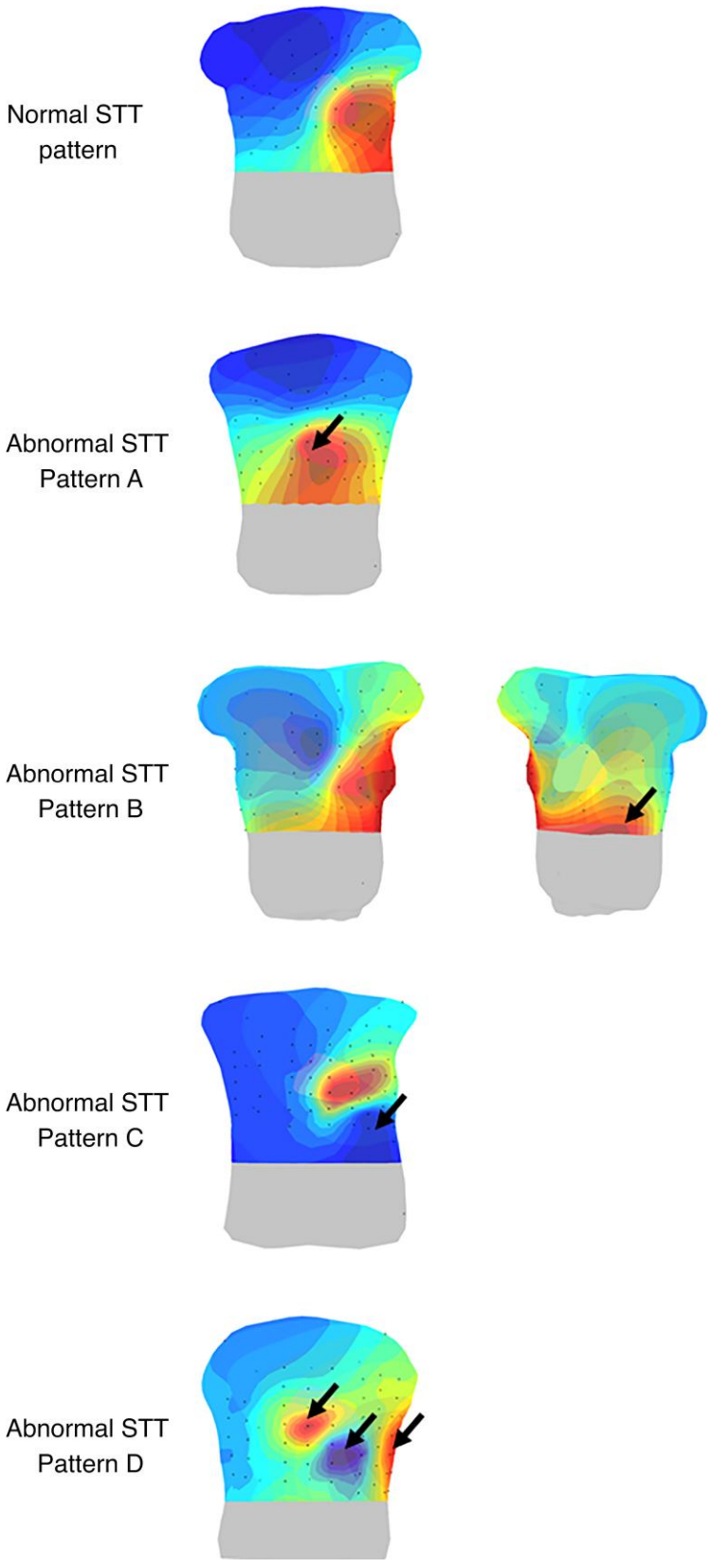

Figure 5 Abnormal STT-patterns in pathogenic plakophilin-2 variant carriers. Isopotential map series are displayed on a 3D model of the heart and torso with electrodes (black dots) for 5 ms intervals within the STT complex. A representative example of a normal STT isopotential map pattern is displayed in row one. Row two till five are representative examples of the four abnormal (black arrows) observed STT-patterns (*A*–*D*) in the *PKP2* population. Dark red indicates the absolute maximum, dark blue the absolute minimum. The isochrones are spaced with equal potential values.

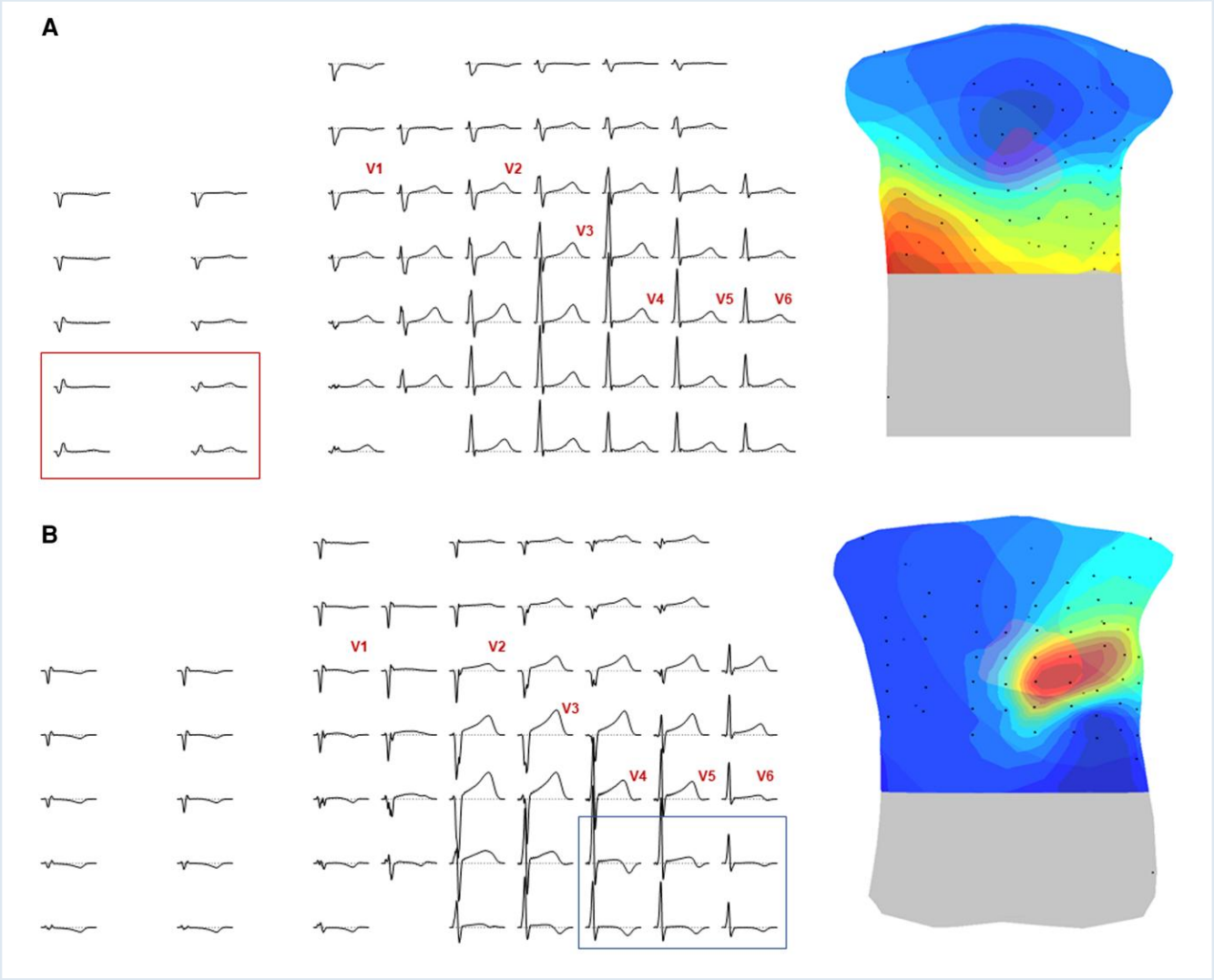

Figure 6 Abnormal electrocardiographic patterns outside the 12 lead ECG configuration. Panel A shows a body surface potential map (left panel) and isopotential map series (right panel) during the depolarization sequence and panel B during the repolarization sequence in two different subjects. Dark red indicates the absolute maximum, dark blue the absolute minimum per time interval. The isochrones are spaced with equal potential values. Black dots represent electrode positions.

masking or neutralization on the QRS/QRST-isopotential map.[18] Hence, this method may result in the loss of resolution, thereby overlooking subtle but important signal characteristics.

In our study, we divided the QRS- and STT-complex into smaller (5 ms) time segments to enable the analysis of subtle ECG waveform changes by isopotential map series. In contrast to the conventionally used 2D-torso representation, we used patient-specific 3D anatomical models of both the torso and the heart, which enabled us to relate cardiac activation and recovery patterns observed on the torso to cardiac anatomy and also electrode positions. This novel method seems very promising because we were able to detect subtle abnormal QRS- and STT-patterns in still pre-clinical pathogenic variant carriers.

Depolarization and repolarization abnormalities were also found in desmosomal variant carriers (*PKP2*, *desmoglein-2 (DSG2)*, *desmocollin-2 (DSC2)*, and *desmoplakin (DSP)*) in studies by Kommata *et al.*[19,20] An abnormal QRS dispersion (>40 ms) was observed in 4/20 desmosomal variant carriers and an abnormal repolarization pattern in 5/20 desmosomal variant carriers.[19,20] They also examined ECG imaging (ECGi)-derived epicardial conduction abnormalities by measuring terminal ventricular activation, defined as epicardial activation during the terminal 20 ms of the QRS complex.[21] Compared to the methods used by Kommata *et al.*, the isopotential map series used in our study may be more sensitive to reveal (local) subtle ECG waveform changes because we analysed spatiotemporal potential distribution in 5 ms intervals throughout the whole QRST complex from the beginning of depolarization to the end of repolarization. Furthermore, the location of ECG waveform changes can be determined with respect to cardiac anatomy and electrode positions. Therefore, more subjects with subtle ECG waveform changes may be identified by isopotential map series. Still, both studies indicate that BSPM is able to detect the presence of an early stage of disease in pre-clinical desmosomal variant carriers. Identification of these early signs of disease in (desmosomal) variant carriers is of utmost importance since electrical remodelling may precede structural and/or functional changes and in some cases ventricular arrhythmias can be the first manifestation of disease.

Abnormal isopotential map series in relation to the 2010 Task Force Criteria

We did not find a homogeneous distribution of observed abnormal QRS- and STT-patterns in a single ARVC stage according to fulfilment of 2010 TFC (*Table 1*), which supports the concept of heterogeneous disease manifestation and progression of ARVC. Also, we did not find a relation between the presence of a specific 2010 TFC and an abnormal QRS-pattern, except for QRS-pattern C (*Table 1*). Subjects with more than two 2010 TFC showing this pattern had a TAD of QRS $\geq$ 55 ms. STT-pattern C (*Table 1*) was related to the presence of negative T-waves, except in three subjects. Two of these subjects, and remarkably also one subject without definite ARVC diagnosis, showed an abnormal negative area on the left distal side of the chest, below the positions of the precordial leads V3–V6 (*Figure 6*, panel B). The other subject showed a large negative area in the leads above the precordial leads V1–V6 and the leads below V1–V2. Furthermore, 7/11 subjects showing STT-pattern C showed a heterogeneous repolarization pattern with multiple minima and maxima at different locations on the torso (*Figure 5*, STT-pattern D). Interestingly, STT-pattern D was observed in six of seven subjects with a history of sustained ventricular arrhythmias. This finding may suggest that subjects showing isopotential maps with multiple minima and maxima may be more vulnerable for ventricular arrhythmias. A study by Kommata *et al.*[21] also confirmed this finding where they observed regional conduction delays in parts of the RV using ECGi.

Possible mechanisms resulting in abnormal isopotential map series

We observed abnormal QRS-patterns most commonly in the leads associated with the RV (84%), both in pre-clinical subjects, borderline, and definite ARVC patients (*Table 1*). The location and timing of the occurring maxima may be related to late ventricular activation of the RV basal segment and/or RV free wall (or RVOT). These locations are in concordance with literature where the apical, basal, and RVOT part of the conventional 'triangle of dysplasia' and more recently the subtricuspid area have been described as the locations of structural involvement in ARVC.[22]

The pathogenesis of ARVC is still not fully understood, but it is hypothesized from mouse model studies that intercalated disk remodeling plays a major role.[5] As desmosomal proteins are part of the intercalated disk, a genetic variant in the desmosomes may lead to redistribution of other intercalated disk proteins resulting in mechanical and electrical uncoupling of cardiac myocytes and thereby decreased conduction velocity. This was also described by Montnach *et al.*[23] where *PKP2* was found to be part of a co-ordinated network of genes involved in calcium regulation and intercellular adhesion. The described mechanisms are hypothesized to induce cell death and inflammation resulting in fibrofatty replacement. However, the described electromechanical uncoupling may occur in the absence of structural heart disease.[24,25] The presence of electromechanical uncoupling prior to cell death and fibrofatty replacement may also explain the difficulty in the detection of early disease.

Abnormal isopotential map series in relation to right ventricular echocardiographic deformation patterns

An interesting finding was that abnormal QRS- and STT-patterns were already present in 7/12 pre-clinical *PKP2*-pathogenic variant carriers with normal RV basal deformation patterns, suggesting that early electrical disease onset may occur before echocardiographic RV deformation abnormalities are present. However, some subjects (4/42) showed an abnormal RV basal deformation pattern while a normal QRS- and/or STT-pattern was observed. Both observations have been reported in literature. Mouse studies indicate the role of a purely electrical mechanism in the early onset of ARVC, whereas Mast *et al.* indicated the presence of mechanical abnormalities in subjects without electrical abnormalities according to the 2010 TFC.[6,25] Further studies in larger patient groups are therefore needed to increase our understanding of the relation between electrical and mechanical changes during disease development.

Limitations

Although this study was limited by a small population size, it is the largest BSPM study in *PKP2*-pathogenic variant carriers to our knowledge. It was therefore not possible to reliably assess significance levels to perform statistical tests on associations. The control population was also small and consisted of subjects with a wide phenotypic variety. The latter may also be considered as a strength of the study since patients with RVOT-PVC and exercise training may mimic an ARVC phenotype.[26]

Future directions

Future studies will focus not only on the inclusion of more subjects but also on the follow-up of all subjects to identify ECG patterns associated with arrhythmic outcomes. Late ventricular activation in the RV basal segment (*Figure 3*, QRS-pattern A) for example was observed among different disease stages of ARVC, even in subjects with definite ARVC suffering from ventricular arrhythmias. This depolarization pattern may therefore hypothetically be characterized as an important depolarization pattern predisposing to ventricular arrhythmias. On the other hand, there were also patterns observed in only a few variant carriers, e.g. STT-pattern B, observed in one pre-clinical variant carrier. It is therefore important to investigate those patterns during disease progression and to relate the observed abnormal QRS- and STT-patterns with arrhythmic outcomes.

Future studies should also investigate the involvement of the left ventricle in early disease onset, both by BSPM and echocardiographic deformation imaging.[22] Also, echocardiographic deformation imaging of other RV segments (mid and apex) should be obtained for comparison with BSPM.[6] Besides echocardiographic deformation imaging, it may also be interesting to compare BSPM with cardiac MRI features like the presence of late gadolinium, increased T1 values and feature tracking CMR.[27,28] Lastly, future research should also focus on the effect of other genetic variants, encoding for desmosomal and non-desmosomal proteins, on BSPM to identify different phenotypical expressions.

Another important aspect of future research is the identification of a disease-specific electrode configuration. Based on QRS-pattern A (*Figure 3*), for example, additional electrodes should be placed at the right distal part of the torso. Late ventricular activation in the basal part of the RV may then be identified (*Figure 6*, panel A). Electrodes may also be positioned below V3–V6 (*Figure 6*, panel B) because two subjects without repolarization abnormalities on the 12 lead ECG showed inverted T-waves on the body surface map below V3–V6. Although the clinical significance of these patterns should be investigated first, the results from this study indicate the importance of a disease-specific electrode positioning outside the standard 12 lead electrode configuration.

Conclusion

By combining isopotential map series with patient-specific 3D anatomical models, cardiac activation and recovery patterns could be related to cardiac anatomy and electrode positions. We were able to observe depolarization and repolarization abnormalities, even in pre-clinical *PKP2*-pathogenic variant carriers with normal deformation patterns

of the sub-tricuspid segment of the RV lateral wall. Furthermore, subtle ECG abnormalities in electrodes outside the standard 12 lead ECG positions could be identified, thereby stressing the importance of disease-specific electrode configurations. Prospective studies are required to identify specific QRS-/STT-patterns that are related to the occurrence of ventricular arrhythmias. In this way, BSPM may aid personalized risk stratification and monitoring of disease progression.

Supplementary material

Supplementary material is available at *Europace* online.

Funding

This work was supported by the Dutch Heart Foundation grant number: QRS-Vision 2018B007, STT-Vision 2020B010, and CVON2015-12 eDETECT.

Conflict of interest: P.M. van Dam is an owner of Peacs BV and ECG-Excellence BV. All remaining authors have declared no conflicts of interest.

Data availability

The data underlying this article will be shared on reasonable request to the corresponding author.

References

1. Groeneweg JA, Bhonsale A, James CA, Te Riele AS, Dooijes D, Tichnell C *et al.* Clinical presentation, long-term follow-up, and outcomes of 1001 arrhythmogenic right ventricular dysplasia/cardiomyopathy patients and family members. *Circ Cardiovasc Genet* 2015;**8**:437–46.
2. Gandjbakhch E, Redheuil A, Pousset F, Charron P, Frank R. Clinical diagnosis, imaging, and genetics of arrhythmogenic right ventricular cardiomyopathy/dysplasia. *J Am Coll Cardiol* 2018;**72**:784–804.
3. Agbaedeng TA, Roberts KA, Colley L, Noubiap JJ, Oxborough D. Incidence and predictors of sudden cardiac death in arrhythmogenic right ventricular cardiomyopathy: a pooled analysis. *Europace* 2022;**24**:1665–74.
4. Bosman LP, Cadrin-Tourigny J, Bourfiss M, Ghasabeh MA, Sharma A, Tichnell C *et al.* Diagnosing arrhythmogenic right ventricular cardiomyopathy by 2010 task force criteria: clinical performance and simplified practical implementation. *Europace* 2020;**22**:787–96.
5. Costa S, Cerrone M, Saguner AM, Brunckhorst C, Delmar M, Duru F. Arrhythmogenic cardiomyopathy: an in-depth look at molecular mechanisms and clinical correlates. *Trends Cardiovasc Med* 2021;**31**:395–402.
6. Mast TP, Taha K, Cramer MJ, Lumens J, van der Heijden JF, Bouma BJ *et al.* The prognostic value of right ventricular deformation imaging in early arrhythmogenic right ventricular cardiomyopathy. *JACC Cardiovasc Imaging* 2019;**12**:446–55.
7. Aengevaeren VL, Froeling M, Hooijmans MT, Monte JR, van den Berg-Faay S, Hopman MTE *et al.* Myocardial injury and compromised cardiomyocyte integrity following a marathon run. *JACC Cardiovasc Imaging* 2020;**13**:1445–7.
8. Moeyersons J, Goovaerts G, Huijghebaert S, Vandenberk B, Willems R, Van Huffel S. Comparison of four different methods for T wave End detection. *Int Jt Conf Biomed Eng Syst Technol* 2017;**10**:92–8.
9. van Dam P, Gordon J, Laks M, Boyle N. Development of new anatomy reconstruction software to localize cardiac isochrones to the cardiac surface from the 12 lead ECG. *J Electrocardiol* 2015;**48**:959–65.
10. Samir A, Kastelein M, van Dam E, van Dam P. Automatic registration of 3D camera recording to model for leads localization. *Comput Cardiol* 2017;**44**:1–4.
11. Teske AJ, De Boeck BWL, Melman PG, Sieswerda GT, Doevendans PA, Cramer MJM. Echocardiographic quantification of myocardial function using tissue deformation imaging, a guide to image acquisition and analysis using tissue Doppler and speckle tracking. *Cardiovasc Ultrasound* 2007;**5**:2–19.
12. Mast TP, Teske AJ, Walmsley J, van der Heijden JF, van Es R, Prinzen FW *et al.* Right ventricular imaging and computer simulation for electromechanical substrate characterization in arrhythmogenic right ventricular cardiomyopathy. *J Am Coll Cardiol* 2016;**68**:2185–97.
13. Kirkels FP, Lie ØH, Cramer MJ, Chivulescu M, Rootwelt-Norberg C, Asselbergs FW *et al.* Right ventricular functional abnormalities in arrhythmogenic cardiomyopathy: association with life-threatening ventricular arrhythmias. *JACC Cardiovasc Imaging* 2021;**14**:900–10.
14. Medvegy M, Duray G, Pintér A, Préda I. Body surface potential mapping: historical background, present possibilities, diagnostic challenges. *Ann Noninvasive Electrocardiol* 2002;**7**:139–51.
15. Widman LE, Liebman J, Thomas C, Fraenkel R, Rudy Y. Electrocardiographic body surface potential maps of the QRS and T of normal young men. Qualitative description and selected quantifications. *J Electrocardiol* 1988;**21**:121–36.
16. Navarcikova S, Sulkova I, Celec P, Hatala R, Urban L, Zlatos L *et al.* Body surface integral maps in patients with arrhythmogenic right ventricular cardiomyopathy. *Bratisl Lek Listy* 2005;**106**:212–5.
17. Peeters HAP, SippensGroenewegen A, Schoonderwoerd BA, Wever EFD, Grimbergen CA, Hauer RNW *et al.* Body-Surface QRST integral mapping. *Circulation* 1997;**95**:2668–76.
18. Medvegy M, Préda I, Savard P, Pintér A, Tremblay G, Nasmith JB *et al.* New body surface isopotential map evaluation method to detect Minor potential losses in non-Q-wave myocardial infarction. *Circulation* 2000;**101**:1115–21.
19. Kommata V, Elshafie M, Sciaraffia E, Perez M, Augustine R, Blomström-Lundqvist C. QRS Dispersion detected in ARVC patients and healthy gene carriers using 252-leads body surface mapping: an explorative study of a potential diagnostic tool for arrhythmogenic right ventricular cardiomyopathy. *Pacing Clin Electrophysiol* 2021;**44**:1355–64.
20. Kommata V, Elshafie M, Blomstrom-Lundquist C. Repolarization abnormalities unmasked with a 252-lead BSM system in patients with ARVC and healthy gene carriers. *Pacing Clin Electrophysiol* 2022;**45**:509–18.
21. Kommata V, Sciaraffia E, Blomström-Lundqvist C. Epicardial conduction abnormalities in patients with arrhythmogenic right ventricular cardiomyopathy (ARVC) and mutation positive healthy family members—A study using electrocardiographic imaging. *PLoS One* 2023;**18**:e0280111.
22. Te Riele AS, James CA, Philips B, Rastegar N, Bhonsale A, Groeneweg JA *et al.* Mutation-positive arrhythmogenic right ventricular dysplasia/cardiomyopathy: the triangle of dysplasia displaced. *J Cardiovasc Electrophysiol* 2013;**24**:1311–20.
23. Montnach J, Agullo-Pascual E, Tadros R, Bezzina CR, Delmar M. Bioinformatic analysis of a plakophilin-2-dependent transcription network: implications for the mechanisms of arrhythmogenic right ventricular cardiomyopathy in humans and in boxer dogs. *Europace* 2018;**20**:125–32.
24. Sato PY, Musa H, Coombs W, Guerrero-Serna G, Patiño GA, Taffet SM *et al.* Loss of plakophilin-2 expression leads to decreased sodium current and slower conduction velocity in cultured cardiac myocytes. *Circ Res* 2009;**105**:523–6.
25. Cerrone M, Montnach J, Lin X, Zhao YT, Zhang M, Agullo-Pascual E *et al.* Plakophilin-2 is required for transcription of genes that control calcium cycling and cardiac rhythm. *Nat Commun* 2017;**8**:106.
26. D'Ascenzi F, Solari M, Corrado D, Zorzi A, Mondillo S. Diagnostic differentiation between arrhythmogenic cardiomyopathy and athlete's heart by using imaging. *JACC Cardiovasc Imaging* 2018;**11**:1327–39.
27. Bourfiss M, Vigneault DM, Aliyari Ghasebeh M, Murray B, James CA, Tichnell C *et al.* Feature tracking CMR reveals abnormal strain in preclinical arrhythmogenic right ventricular dysplasia/cardiomyopathy: a multisoftware feasibility and clinical implementation study. *J Cardiovasc Magn Reson* 2017;**19**:66.
28. Bourfiss M, Prakken NHJ, van der Heijden JF, Kamel I, Zimmerman SL, Asselbergs FW *et al.* Diagnostic value of native T1 mapping in arrhythmogenic right ventricular cardiomyopathy. *JACC Cardiovasc Imaging* 2019;**12**:1580–2.